ACS Photonics

pubs.acs.org/journal/apchd5 Article

Topological Band Gaps Enlarged in Epsilon-Near-Zero Magneto-Optical Photonic Crystals

Tianji Liu,* Nobukiyo Kobayashi, Kenji Ikeda, Yasutomo Ota,* and Satoshi Iwamoto*

Cite This: *ACS Photonics* 2022, 9, 1621−1626 Read Online

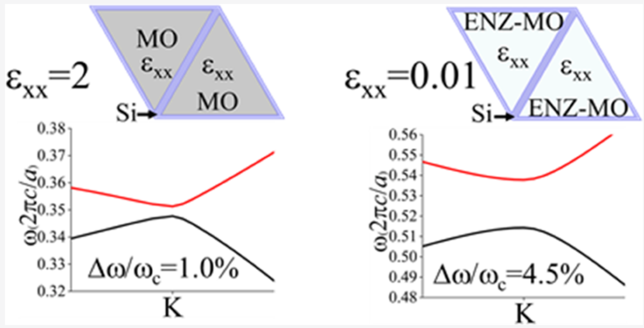

ABSTRACT: Topological photonics provides exciting and emerging opportunities for the manipulation of light. As the photonic analogue of quantum Hall edge states, chiral edge modes, arising at the interface between two photonic topological structures with different Chern numbers, hold great promise for robust transport of light against disorders and defects. However, for magneto-optical material-based topological photonic crystals, the transport performance of chiral edge modes is strongly dependent on the topological gap sizes, which are usually very narrow at optical frequencies due to the lack of magneto-optical materials with strong nonreciprocal responses. Here, we numerically demonstrated that the introduction of an epsilon-near-zero effect to magneto-optical photonic crystals could remarkably enlarge topological gap sizes due to the boosted magneto-optical response. Eigenmode calculation results show that the boosted magneto-optical response correlates to the enhanced nonreciprocal power flows in magnetized photonic crystals with an epsilon-near-zero diagonal permittivity. The enlarged topological band gap leads to the broadband and well-confined chiral edge modes propagating along the magnetized boundary between two oppositely magnetized photonic crystals. More importantly, such mode propagation shows strong robustness against sharp bends and large defects. In principle, our proposal for the enlargement of topological photonic band gaps could also be valid in photonic crystal slabs or even three-dimensional photonic crystals. Our results not only suggest the possibility to improve the transport performance of one-way modes in magneto-optical photonic crystals but also enrich the physical understanding of the epsilon-near-zero effect-based topological photonics.

KEYWORDS: *topological band gap, chiral edge modes, magneto-optical effect, epsilon-near-zero effect, one-way waveguide*

■ INTRODUCTION

As an emerging research area, a plethora of exotic and intriguing phenomena have been explored in topological photonics.[1−3] In their seminal works, Haldane and Raghu pointed out that backscattering-immune chiral edge modes (CEMs) are obtainable at the domain wall between two topologically distinct two-dimensional (2D) magnetized photonic crystals (PhCs).[4,5] The unidirectionality and robustness of CEMs result from the breaking of time-reversal symmetry (TRS) and the associated nontrivial topological bands using magneto-optical (MO) materials. In principle, the robustness of CEMs is strongly dependent on the obtainable topological gap sizes.[6] When topological gap sizes are small, edge modes are susceptible to scattering to bulk modes once large defects arise near topological domain walls. So far, many theoretical and experimental advances have been reported for realizing robust CEMs (or one-way modes) at microwave frequencies,[6−10] benefited from large topological gap sizes supported by gyromagnetic PhCs with large off-diagonal permeability.[11] In contrast, only extremely narrow topological gaps were numerically and experimentally demonstrated at optical frequencies (e.g., <50 pm at 1.55 μm wavelength[12,13]) due to the lack of gyrotropic materials with large off-diagonal permittivity or permeability. Although edge modes were observed in topological nanostructures,[12−14] their robustness against strong disorders or defects is unknown. Furthermore, narrow topological gaps lead to poor field confinement for CEMs, hindering the development of high-density topological photonic integrated circuits. Therefore, to obtain robust, broadband, and well-confined CEMs at optical frequencies, it is necessary to enlarge topological gap sizes. In the area of nanophotonics, one can utilize plasmonic or dielectric metastructures to enhance Faraday rotation or Kerr rotation.[15−17] In addition, benefitting from the vanishing permittivity, the strong enhancement of optical nonlinearity,[18−23] nonlocality,[24] and chirality[25] have been expected near the epsilon-near-zero (ENZ) wavelength. ENZ slabs or metamaterials are also well-

Received: December 17, 2021
Published: April 27, 2022

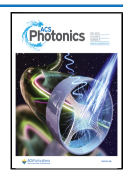

https://doi.org/10.1021/acsphotonics.1c01942
ACS Photonics 2022, 9, 1621−1626

known for manipulating the flow of light, such as electromagnetic wave tunneling through distorted channels,[26] tailoring the radiation phase pattern,[27] efficient vortex generation,[28] and enhancing asymmetric transmission.[29] Recently, enhanced MO effects were observed in hyperbolic metamaterials at ENZ wavelengths.[30,31] Materials with both ENZ property and MO responses, i.e., ENZ-MO materials, play an important role in various applications, such as nonreciprocal transmission,[32] optical isolation,[33] unidirectional mode propagation,[34,35] and circulation-dependent sources.[36] However, the application of ENZ-MO materials for enlarging the sizes of topological photonic band gaps has not yet been investigated so far.

In this paper, we numerically demonstrated that ENZ-MO material-based topological PhCs (ENZ-MO PhCs) enable the enlargement of topological gap sizes. The investigated PhC is composed of a honeycomb lattice of MO triangular prisms in an infinite thick Si slab. We found that topological gap sizes are monotonously increased with the reduction of diagonal permittivity in MO prisms, especially in the ENZ region. Such enlarged topological gaps result from the boosted nonreciprocal light−matter interaction in MO PhCs related to the strong electric field enhancement and the large circulation of nonreciprocal power flows in ENZ areas. Furthermore, robust, well-confined, and unidirectional modes with significant field enhancement are supported by our one-way waveguides, which are composed of two oppositely magnetized ENZ-MO PhCs. Note that although 2D PhCs are discussed here, ENZ-MO materials are still valid for the enlargement of topological gaps in PhC slabs or even three-dimensional (3D) PhCs. Our results may provide a promising approach to improving the performance of one-way waveguides at optical frequencies.

■ RESULTS AND DISCUSSION

Figure 1a shows a unit cell of the investigated 2D PhCs with a honeycomb lattice, which preserves spatial-inversion symmetry

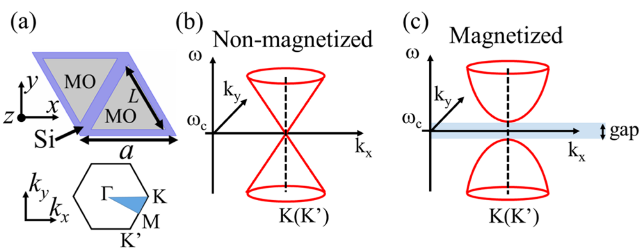

Figure 1. (a) Unit cell of investigated 2D MO PhC with honeycomb lattice (top) and the corresponding Brillouin zone (bottom), the colored area at the bottom is the irreducible Brillouin zone. (b) Band diagram near $K(K')$-point without magnetization. (c) Band diagram near $K(K')$-point with magnetization.

(SIS). In the unit cell, two MO equilateral triangular prisms (gray areas in Figure 1a) are embedded into a high-index infinite thick Si slab. The filling ratio of MO prisms is defined as $f = (L/a)^2$, L is the side length of equilateral triangular prisms and a is the lattice constant of PhCs. For simplicity, dispersionless and lossless materials are assumed throughout this paper. The Si slab has a scalar relative permittivity of 12 and MO triangular prisms have an antisymmetric complex relative permittivity tensor $\hat{\varepsilon}_{\rm MO}$. For z-direction magnetized MO materials, $\hat{\varepsilon}_{\rm MO}$ has the form

$$\hat{\varepsilon}_{\rm MO} = \begin{pmatrix} \varepsilon_{xx} & -i\Lambda & 0 \\ i\Lambda & \varepsilon_{yy} & 0 \\ 0 & 0 & \varepsilon_{zz} \end{pmatrix} \tag{1}$$

the magnetized ENZ-MO materials can be defined by the combination of $0 < \varepsilon_{xx} = \varepsilon_{yy} = \varepsilon_{zz} < 1$ and $\Lambda \neq 0$. Note the topological properties of MO PhCs here is independent of ε_{zz}. We fixed $\Lambda = \pm 0.1$ and $f = 0.81$ (i.e., $L/a = 0.9$) for all magnetized PhCs, all calculations are performed using the finite-element method-based software package COMSOL Multiphysics. In the experiment, hyperbolic metamaterials and the low-loss indium tin oxide are possible candidates for ENZ-MO materials;[30,31,37] furthermore, using ferromagnetic nanogranular materials may obtain a large Λ.[38−40] Figure 1b,c shows schematic band structures of MO-based 2D honeycomb PhCs near Brillouin zone corners without and with magnetization, respectively. Without magnetization ($\Lambda = 0$), $\hat{\varepsilon}_{\rm MO}$ is reduced to a scalar relative permittivity and the PhC preserves SIS and TRS. As a result, the first and second bands for transverse electric (TE) polarization deterministically touch each other at the corners of the first Brillouin zone, i.e., at K and K'-points shown in the bottom panel of Figure 1a, forming the so-called photonic Dirac points. Hence, the nontrivial topological band gap is zero no matter the value of ε_{xx}, see Figure S1 in Supporting Information for details. Here, TE polarization is defined as the zero out-of-plane component of electric fields. The coexistence of SIS and TRS leads to zero Berry curvatures in the entire 2D reciprocal space, except for Dirac points where they are ill-defined.[4,5] With magnetization ($\Lambda \neq 0$), the antisymmetric off-diagonal elements of $\hat{\varepsilon}_{\rm MO}$ break the TRS and lift the band degeneracy at Dirac points, opening a MO coupling induced topological gap ($\Delta\omega$) at the $K(K')$-point in Figure 1c. Importantly, the broken TRS leads to the even symmetry of Berry curvatures in the reciprocal space and associated nonzero Chern numbers for two photonic bands, indicating the topologically nontrivial property of photonic bands.

To investigate the impact of ε_{xx} in MO PhCs, we directly compared two band diagrams of PhCs with $\varepsilon_{xx} = 2$ and $\varepsilon_{xx} = 0.01$, respectively (Figure 2). For the PhC with $\varepsilon_{xx} = 2$, a complete topological gap but only a 1.0% gap−mid-gap ratio ($\Delta\omega/\omega_c$) is obtained (Figure 2a,b), ω_c is the mid-gap frequency. In contrast, a complete and enlarged topological gap with $\Delta\omega/\omega_c = 4.5\%$ below the light line is obtained when $\varepsilon_{xx} = 0.01$ (Figure 2d,e). The topological gap size corresponds to 69 nm at 1.55 μm wavelength and is much larger than the reported ∼40 pm topological gap using yttrium iron garnet-based PhCs.[12] To explain the large topological gap sizes that appeared in ENZ-MO PhCs, we picked two representative points A and B at the first TE bands at $K(K')$-points for $\varepsilon_{xx} = 2$ (Figure 2b) and $\varepsilon_{xx} = 0.01$ (Figure 2e), respectively. The corresponding eigenmode profiles of points A and B are shown in Figure 2c,f. Weak electric fields (E-fields) at point A are poorly confined within MO prisms (Figure 2c). Although time-averaged Poynting vectors exhibit nonreciprocal patterns (yellow arrows in Figure 2c), a majority of clockwise and counterclockwise power flows cancel each other and result in the small net circulation of nonreciprocal rotating power flows, indicating the weak nonreciprocal MO effect in the PhC. Note the weak nonreciprocal interaction correlates to small topological gap sizes, due to the small MO coupling strength between two eigenmodes from the first and the second bands

https://doi.org/10.1021/acsphotonics.1c01942
ACS Photonics 2022, 9, 1621−1626

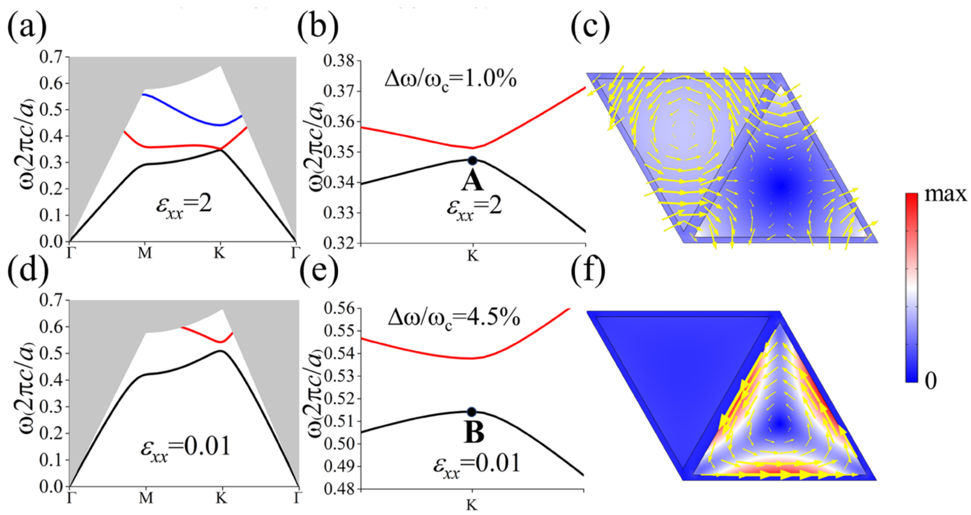

Figure 2. Calculation results of 2D MO-based PhC with $\varepsilon_{xx} = 2$ (a−c) and $\varepsilon_{xx} = 0.01$ (d−f), respectively. c is the light speed in a vacuum. (a, d) TE band diagrams for $\varepsilon_{xx} = 2$ (a) and $\varepsilon_{xx} = 0.01$ (d). (b, e) Enlarged band diagrams near K-points, A point (b), and B point (e) are picked at both K-points of the first TE bands for $\varepsilon_{xx} = 2$ and $\varepsilon_{xx} = 0.01$, respectively. (c, f) Amplitudes of E-fields at A point (c) and B point (f). Yellow arrows indicate the direction of time-averaged Poynting vectors.

at $K(K')$-point.[41−43] On the contrary, remarkably enhanced E-fields and large circulation of rotating power flow at point B are well-confined within MO triangular prisms, as shown in Figure 2f, indicating the enhancement of MO coupling between two eigenmodes at $K(K')$ points and the associated enlargement of the topological gap size. The above comparison clearly shows the important role of the ENZ effect in the enhancement of MO responses in our PhCs. Importantly, the enlarged topological gap size and the large circulation of nonreciprocal power flow still survive when lossy ENZ-MO materials are used, see Figure S2 in the Supporting Information.

To quantitatively indicate the relationship between topological gap sizes and ε_{xx}, the variation of $\Delta\omega/\omega_c$ for ε_{xx} is calculated and shown in Figure 3. $\Delta\omega/\omega_c$ is monotonously

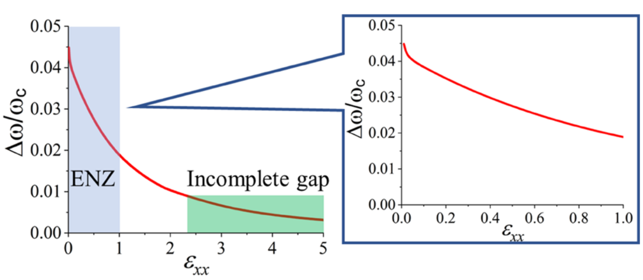

Figure 3. Variation of $\Delta\omega/\omega_c$ for ε_{xx}. The right inset is the enlarged view for the ENZ region.

increased when ε_{xx} is reduced. For $\varepsilon_{xx} > 2.3$ (green shaded area in Figure 3), the incomplete and insufficient gap would limit the transport performance of CEMs. For the ENZ region ($0.01 < \varepsilon_{xx} < 1$), see the blue shaded area and the inset on the right-hand side of Figure 3, a gradually increased $\Delta\omega/\omega_c$ is shown, due to the enhanced nonreciprocal light−matter interaction. Note $\Delta\omega/\omega_c = 4.5\%$ obtained at $\varepsilon_{xx} = 0.01$ is not the ultimate limit for our ENZ-MO PhCs, larger $\Delta\omega/\omega_c$ can be expected when ε_{xx} is further reduced. Except for the fixed $\Lambda = 0.1$, we also calculated the variation of $\Delta\omega/\omega_c$ for ε_{xx} with different Λ values, see Figure S3 in the Supporting Information for details.

As shown in Figure 4a−c, mode characteristics of CEMs are analyzed in two oppositely magnetized domains of ENZ-MO PhCs. In Figure 4a, MO triangular prisms in dark red and dark blue areas indicate $\Lambda = +0.1$ and $\Lambda = -0.1$, respectively; two areas are separated by a magnetized boundary labeled by a green line. In calculation, a supercell containing 20 primitive unit cells is used, i.e., 10 cells with $\Lambda = +0.1$ and 10 cells with $\Lambda = -0.1$, respectively. The periodic condition is used along with x- and y-directions. Two CEMs can be found in projected band diagrams (Figure 4b,c), such modes are photonic analogues of the Jackiw−Rebbi edge states at the magnetized boundary.[44−46] Note we removed the other two CEMs arising at the top or bottom boundary because they are just the spatial copies of the above two CEMs. The number of CEMs corresponds to the gap Chern number difference between two magnetized MO PhCs (ΔC), i.e., $\Delta C = C_1(\Lambda = 0.1) - C_1(\Lambda = -0.1) = 1-(-1) = 2$, C_1 ($\Lambda = \pm 0.1$) is the Chern number of the first band with $\Lambda = \pm 0.1$. Here, we adopted a numerical method to calculate C_1, calculation details are not shown in this paper, which is well-explained in ref 47, 48. The unidirectionality of CEMs can be found from the same sign of slopes of red curves (within the bulk gap) in Figure 4b,c. Again, in contrast to the PhC with $\varepsilon_{xx} = 2$ (Figure 4b), the topological gap size is much enlarged for the ENZ-MO PhC with $\varepsilon_{xx} = 0.01$ (Figure 4c), providing the broad frequency band for the transport of CEMs. As a reference, the projected band structure without magnetization is also calculated ($\varepsilon_{xx} = 0.01$, $\Lambda = 0$), neither topological band gaps nor CEMs exist, see Figure S4 in the Supporting Information.

To understand the transport properties of one-way modes in topological PhCs with the above magnetized configurations (Figure 4d), we calculated TE mode profiles (square of the z-component of magnetic fields: $|H_z|^2$) in straight one-way waveguides with $\varepsilon_{xx} = 2$ (Figure 4e) and $\varepsilon_{xx} = 0.01$ (Figure 4f), respectively. Such waveguides are composed of 10,000 (100 × 100) primitive unit cells and the open boundary condition is used for the outermost boundaries. One-way modes are excited by a circularly polarized dipole source near the magnetized boundary (red dot in Figure 4d), such modes are formed by the interference of two CEMs in Figure 4b,c. One should note

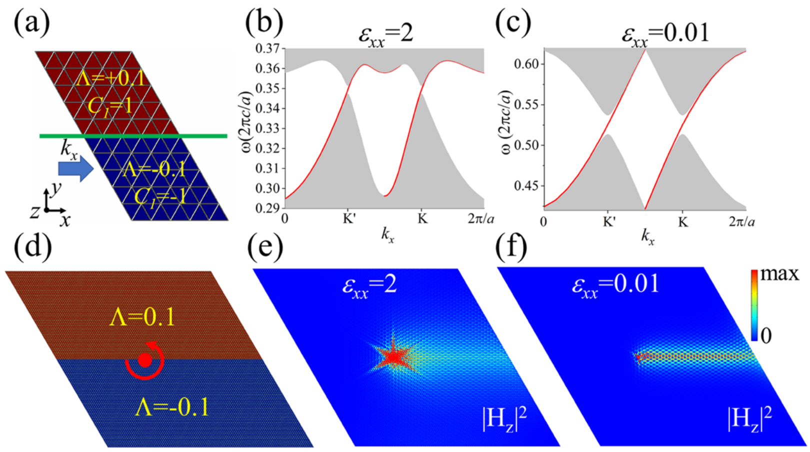

Figure 4. (a) Schematic view of the investigated MO PhCs. The green line indicates the magnetized boundary. (b, c) Projected band structures for MO PhCs with $\varepsilon_{xx} = 2$ (b) and $\varepsilon_{xx} = 0.01$ (c), respectively. (d) Schematic view of the straight one-way waveguide. The red dot indicates a circular dipole source near the edge. (e, f) Transport of one-way modes with $\varepsilon_{xx} = 2$ (e) and $\varepsilon_{xx} = 0.01$ (f), respectively. Note color bars are not unified in (e, f); fields in (f) are orders of magnitude larger than fields in (e).

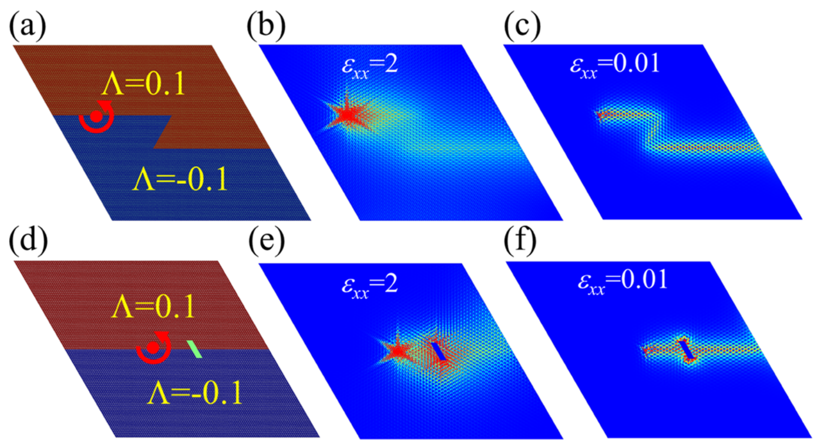

Figure 5. (a) Schematic view of Z-shaped one-way waveguides. (b, c) Transport of one-way modes in Z-shaped waveguides with $\varepsilon_{xx} = 2$ (b) and $\varepsilon_{xx} = 0.01$ (c). (d) Schematic view of straight one-way waveguides with a PEC defect; the green parallelogram indicates the PEC defect. (e, f) Transport of one-way modes in straight waveguides with a PEC defect for $\varepsilon_{xx} = 2$ (e) and $\varepsilon_{xx} = 0.01$ (f).

the unidirectionality of one-way modes is unchanged no matter linearly, circularly, or elliptically polarized sources are used, see Figure S5 in the Supporting Information for the detailed discussion. For PhC with $\varepsilon_{xx} = 2$ at $\omega_0 = \omega_c = 0.3495(2\pi c/a)$, the lateral field confinement of one-way modes is relatively poor and the skin depth (i.e., the depth for $|H_z|^2$ reduced to $1/e$) is $13.1a$ (Figure 4e). Additionally, the star-like radiation pattern can be observed near the position of the circular dipole source due to the long penetration length of evanescent modes in PhCs with a small gap. Neither the poor field confinement nor the penetrated radiation is favorable for high-density topological photonic integrated circuits. The transmittance for one-way waveguides with $\varepsilon_{xx} = 2$ is only 69.7%. Here, the transmittance is defined by the ratio of the power outflow through the right-side boundary to the total power outflow. In other words, around 30% of the total optical power is leaked from the left, top, and bottom boundaries of the calculated domain. The low transmittance results from the large power leakage at the outer boundaries, which can be improved by the enlargement of the calculated domain. In stark contrast, well-confined and one-way modes with significant field enhancement are found for the waveguide with $\varepsilon_{xx} = 0.01$ at $\omega_0 = \omega_c = 0.525(2\pi c/a)$, as shown in Figure 4f. Additionally, the radiation pattern near the circular dipole source disappears due to the suppressed penetration in ENZ-MO PhCs with a large gap. Benefitting from the enlarged topological gap in the PhC with $\varepsilon_{xx} = 0.01$, the skin depth is $3.6a$ and the transmittance is 99.9%, both parameters are greatly improved from the PhC with $\varepsilon_{xx} = 2$. Within the topological gap ranging from $0.514(2\pi c/a)$ to $0.537(2\pi c/a)$, the transmittance is above 99% (the spectrum is not shown), indicating the near-perfect broadband transport in the ENZ-MO PhC.

To evaluate the robustness against defects or disorders for one-way modes, we analyzed Z-shaped waveguides (Figure 5a−c) and straight waveguides with perfect electric conductor (PEC) defects (Figure 5d−f), respectively. Again, the geometry of one-way waveguides can be defined by the magnetized boundary between two oppositely magnetized areas (Figure 5a,d). One-way modes are shown in Z-shaped waveguides with $\varepsilon_{xx} = 2$ (Figure 5b) and $\varepsilon_{xx} = 0.01$ (Figure 5c), their robustness against two 120° sharp bends can be observed from $|H_z|^2$ profiles. No backscattering mode is found in the case of $\varepsilon_{xx} = 2$ (Figure 5b). However, the poor confinement and the strong penetration near the source still exist, leading to only 43.1% transmittance. For the ENZ-MO PhC with $\varepsilon_{xx} = 0.01$ (Figure 5c), well-confined one-way modes

https://doi.org/10.1021/acsphotonics.1c01942
ACS Photonics 2022, 9, 1621−1626

with 99.5% power transmittance show their robustness against sharp bends. In Figure 5d, a PEC parallelogram slab with the size of $3a \times 10a$ is introduced at the position $20a$ away from the circular dipole source (the green area in Figure 5d). Again, for the PhC with $\varepsilon_{xx} = 0.01$, well-confined and enhanced one-way modes with 99.9% transmittance are obtained (Figure 5f), indicating sufficient robustness against the large-sized PEC defect. In contrast, for the MO PhC with $\varepsilon_{xx} = 2$, the transportation of one-way modes deviates from the magnetized boundary, indicating insufficient robustness against the PEC defect (Figure 5e).

■ CONCLUSIONS

We numerically demonstrated that the introduction of the ENZ effect is responsible for the enhancement of MO responses and the associated enlargement of topological gaps for topological MO PhCs. Benefitting from the enlarged topological gap sizes, broadband and well-confined one-way modes are obtained in ENZ-MO PhCs, exhibiting strong robustness against sharp bends and large-sized PEC defects. Our results not only manifest the possibility to improve the transportation of CEMs at optical frequencies but also provide new opportunities for many applications of photonic topological insulators with broken TRS, such as topological splitters,[8,49] nonreciprocal lasers,[12] and coherent topological light sources.[13]

■ METHODS

All calculations are performed using the finite-element method-based software package COMSOL Multiphysics. For band structures and eigenmodes calculations (Figures 2−4b,c and S1−S4), Floquet periodic boundary conditions and eigenfrequency study steps are used for solving linear eigenvalue problems. Free triangular meshing with a maximum size of $0.04a$ is adopted in the division of finite elements. For chiral edge modes propagation calculations (Figures 4e,f, 5, and S5), scattering boundary conditions (similar to the Sommerfeld radiation condition) and frequency domain study steps are used. Free triangular meshing with a maximum size of $0.08a$ is adopted in the division of finite elements.

■ ASSOCIATED CONTENT

Supporting Information

The Supporting Information is available free of charge at https://pubs.acs.org/doi/10.1021/acsphotonics.1c01942.

Photonic band structures without magnetization; topological band structures with lossy ENZ-MO materials; variation of topological gap sizes for ε_{xx} with different Λ; projected band structures without magnetization; and one-way modes excited by different polarized dipole sources (PDF)

■ AUTHOR INFORMATION

Corresponding Authors

Tianji Liu − *Research Center for Advanced Science and Technology, The University of Tokyo, Tokyo 153-8505, Japan; GPL Photonics Laboratory, State Key Laboratory of Applied Optics, Changchun Institute of Optics, Fine Mechanics and Physics, Chinese Academy of Sciences, Changchun 130033, China;* orcid.org/0000-0002-5862-2449; Email: liu-tj@iis.u-tokyo.ac.jp

Yasutomo Ota − *Department of Applied Physics and Physico-Informatics, Keio University, Yokohama 223-8522, Japan; Institute for Nano Quantum Information Electronics, The University of Tokyo, Tokyo 153-8505, Japan*; Email: ota@appi.keio.ac.jp

Satoshi Iwamoto − *Research Center for Advanced Science and Technology, Institute for Nano Quantum Information Electronics, and Institute of Industrial Science, The University of Tokyo, Tokyo 153-8505, Japan;* orcid.org/0000-0001-9805-6325; Email: iwamoto@iis.u-tokyo.ac.jp

Authors

Nobukiyo Kobayashi − *Research Institute for Electromagnetic Materials, Tomiya 981-3341, Japan*

Kenji Ikeda − *Research Institute for Electromagnetic Materials, Tomiya 981-3341, Japan*

Complete contact information is available at: https://pubs.acs.org/10.1021/acsphotonics.1c01942

Funding

This work was supported by JST-CREST (JPMJCR19T1), JSPS KAKENHI (17H03420, 17H06138, 17K06849, 19K05300, and 19K21959) and the Nippon Sheet Glass Foundation for Materials Science and Engineering.

Notes

The authors declare no competing financial interest.

■ REFERENCES

(1) Lu, L.; Joannopoulos, J. D.; Soljačić, M. Topological Photonics. *Nat. Photonics* **2014**, *8*, 821−829.
(2) Khanikaev, A. B.; Shvets, G. Two-Dimensional Topological Photonics. *Nat. Photonics* **2017**, *11*, 763−773.
(3) Ozawa, T.; Price, H. M.; Amo, A.; Goldman, N.; Hafezi, M.; Lu, L.; Rechtsman, M. C.; Schuster, D.; Simon, J.; Zilberberg, O.; et al. Topological Photonics. *Rev. Mod. Phys.* **2019**, *91*, No. 015006.
(4) Haldane, F. D. M.; Raghu, S. Possible Realization of Directional Optical Waveguides in Photonic Crystals with Broken Time-Reversal Symmetry. *Phys. Rev. Lett.* **2008**, *100*, No. 013904.
(5) Raghu, S.; Haldane, F. D. M. Analogs of Quantum-Hall-Effect Edge States in Photonic Crystals. *Phys. Rev. A* **2008**, *78*, No. 033834.
(6) Wang, Z.; Chong, Y. D.; Joannopoulos, J. D.; Soljačić, M. Reflection-Free One-Way Edge Modes in a Gyromagnetic Photonic Crystal. *Phys. Rev. Lett.* **2008**, *100*, No. 013905.
(7) Wang, Z.; Chong, Y.; Joannopoulos, J. D.; Soljačić, M. Observation of Unidirectional Backscattering-Immune Topological Electromagnetic States. *Nature* **2009**, *461*, 772−775.
(8) Skirlo, S. A.; Lu, L.; Igarashi, Y.; Yan, Q.; Joannopoulos, J.; Soljačić, M. Experimental Observation of Large Chern Numbers in Photonic Crystals. *Phys. Rev. Lett.* **2015**, *115*, No. 253901.
(9) Poo, Y.; Wu, R.; Lin, Z.; Yang, Y.; Chan, C. T. Experimental Realization of Self-Guiding Unidirectional Electromagnetic Edge States. *Phys. Rev. Lett.* **2011**, *106*, No. 093903.
(10) Wang, M.; Zhang, R. Y.; Zhang, L.; Wang, D.; Guo, Q.; Zhang, Z. Q.; Chan, C. T. Topological One-Way Large-Area Waveguide States in Magnetic Photonic Crystals. *Phys. Rev. Lett.* **2021**, *126*, No. 067401.
(11) Pozar, D. M. *Microwave Engineering*, 4th ed.; Wiley, 2011.
(12) Bahari, B.; Ndao, A.; Vallini, F.; Amili, A. El.; Fainman, Y.; Kanté, B. Nonreciprocal Lasing in Topological Cavities of Arbitrary Geometries. *Science* **2017**, *358*, 636−640.
(13) Bahari, B.; Hsu, L.; Pan, S. H.; Preece, D.; Ndao, A.; El Amili, A.; Fainman, Y.; Kanté, B. Photonic Quantum Hall Effect and Multiplexed Light Sources of Large Orbital Angular Momenta. *Nat. Phys.* **2021**, *17*, 700−703.

(14) Ota, Y.; Takata, K.; Ozawa, T.; Amo, A.; Jia, Z.; Kante, B.; Notomi, M.; Arakawa, Y.; Iwamoto, S. Active Topological Photonics. *Nanophotonics* **2020**, *9*, 547−567.

(15) Chin, J. Y.; Steinle, T.; Wehlus, T.; Dregely, D.; Weiss, T.; Belotelov, V. I.; Stritzker, B.; Giessen, H. Nonreciprocal Plasmonics Enables Giant Enhancement of Thin-Film Faraday Rotation. *Nat. Commun.* **2013**, *4*, No. 1599.

(16) Bsawmaii, L.; Gamet, E.; Royer, F.; Neveu, S.; Jamon, D. Longitudinal Magneto-Optical Effect Enhancement with High Transmission through a 1D All-Dielectric Resonant Guided Mode Grating. *Opt. Express* **2020**, *28*, 8436−8444.

(17) Loughran, T. H. J.; Keatley, P. S.; Hendry, E.; Barnes, W. L.; Hicken, R. J. Enhancing the Magneto-Optical Kerr Effect through the Use of a Plasmonic Antenna. *Opt. Express* **2018**, *26*, 4738−4750.

(18) Liberal, I.; Engheta, N. Near-Zero Refractive Index Photonics. *Nat. Photonics* **2017**, *11*, 149−158.

(19) Rizza, C.; Ciattoni, A.; Palange, E. Two-Peaked and Flat-Top Perfect Bright Solitons in Nonlinear Metamaterials with Epsilon near Zero. *Phys. Rev. A* **2011**, *83*, No. 053805.

(20) Ciattoni, A.; Rizza, C.; Palange, E. Transverse Power Flow Reversing of Guided Waves in Extreme Nonlinear Metamaterials. *Opt. Express* **2010**, *18*, 11911−11916.

(21) Ciattoni, A.; Rizza, C.; Palange, E. Transmissivity Directional Hysteresis of a Nonlinear Metamaterial Slab with Very Small Linear Permittivity. *Opt. Lett.* **2010**, *35*, 2130−2132.

(22) Vincenti, M. A.; De Ceglia, D.; Ciattoni, A.; Scalora, M. Singularity-Driven Second- and Third-Harmonic Generation at ε-near-Zero Crossing Points. *Phys. Rev. A* **2011**, *84*, No. 063826.

(23) Reshef, O.; De Leon, I.; Alam, M. Z.; Boyd, R. W. Nonlinear Optical Effects in Epsilon-near-Zero Media. *Nat. Rev. Mater.* **2019**, *4*, 535−551.

(24) Pollard, R. J.; Murphy, A.; Hendren, W. R.; Evans, P. R.; Atkinson, R.; Wurtz, G. A.; Zayats, A. V.; Podolskiy, V. A. Optical Nonlocalities and Additional Waves in Epsilon-near-Zero Metamaterials. *Phys. Rev. Lett.* **2009**, *102*, No. 127405.

(25) Rizza, C.; Di Falco, A.; Scalora, M.; Ciattoni, A. One-Dimensional Chirality: Strong Optical Activity in Epsilon-Near-Zero Metamaterials. *Phys. Rev. Lett.* **2015**, *115*, No. 057401.

(26) Silveirinha, M.; Engheta, N. Tunneling of Electromagnetic Energy through Subwavelength Channels and Bends Using ε-near-Zero Materials. *Phys. Rev. Lett.* **2006**, *97*, No. 157403.

(27) Alù, A.; Silveirinha, M. G.; Salandrino, A.; Engheta, N. Epsilon-near-Zero Metamaterials and Electromagnetic Sources: Tailoring the Radiation Phase Pattern. *Phys. Rev. B* **2007**, *75*, No. 155410.

(28) Ciattoni, A.; Marini, A.; Rizza, C. Efficient Vortex Generation in Subwavelength Epsilon-Near-Zero Slabs. *Phys. Rev. Lett.* **2017**, *118*, No. 104301.

(29) Rizza, C.; Li, X.; Di Falco, A.; Palange, E.; Marini, A.; Ciattoni, A. Enhanced Asymmetric Transmission in Hyperbolic Epsilon-near-Zero Slabs. *J. Opt.* **2018**, *20*, No. 085001.

(30) Kolmychek, I. A.; Pomozov, A. R.; Leontiev, A. P.; Napolskii, K. S.; Murzina, T. V. Magneto-Optical Effects in Hyperbolic Metamaterials. *Opt. Lett.* **2018**, *43*, 3917−3920.

(31) Kolmychek, I. A.; Pomozov, A. R.; Novikov, V. B.; Leontiev, A. P.; Napolskii, K. S.; Murzina, T. V. Anomalous Birefringence and Enhanced Magneto-Optical Effects in Epsilon-near-Zero Metamaterials Based on Nanorods' Arrays. *Opt. Express* **2019**, *27*, 32069−32074.

(32) Guo, Z.; Wu, F.; Xue, C.; Jiang, H.; Sun, Y.; Li, Y.; Chen, H. Significant Enhancement of Magneto-Optical Effect in One-Dimensional Photonic Crystals with a Magnetized Epsilon-near-Zero Defect. *J. Appl. Phys.* **2018**, *124*, No. 103104.

(33) Davoyan, A. R.; Mahmoud, A. M.; Engheta, N. Optical Isolation with Epsilon-near-Zero Metamaterials. *Opt. Express* **2013**, *21*, 3279−3286.

(34) Davoyan, A. R.; Engheta, N. Theory of Wave Propagation in Magnetized Near-Zero-Epsilon Metamaterials: Evidence for One-Way Photonic States and Magnetically Switched Transparency and Opacity. *Phys. Rev. Lett.* **2013**, *111*, No. 257401.

(35) Horsley, S. A. R. Unidirectional Wave Propagation in Media with Complex Principal Axes. *Phys. Rev. A* **2018**, *97*, No. 023834.

(36) Horsley, S. A. R.; Woolley, M. Zero-Refractive-Index Materials and Topological Photonics. *Nat. Phys.* **2021**, *17*, 348−355.

(37) Ikeda, K.; Liu, T.; Ota, Y.; Iwamoto, S.; Kobayashi, N. Magneto-Optical Effect of ITO Films as Epsilon-near-Zero Materials, *The 82nd JSAP Autumn Meeting 2021*; 13p-N321-15, 2021.

(38) Kobayashi, N.; Ikeda, K.; Gu, B.; Takahashi, S.; Masumoto, H.; Maekawa, S. Giant Faraday Rotation in Metal-Fluoride Nanogranular Films. *Sci. Rep.* **2018**, *8*, No. 4978.

(39) Kobayashi, N.; Masumoto, H.; Takahashi, S.; Maekawa, S. Optically Transparent Ferromagnetic Nanogranular Films with Tunable Transmittance. *Sci. Rep.* **2016**, *6*, No. 34227.

(40) Ikeda, K.; Kobayashi, N.; Arai, K.-I. Large Faraday Effect in Nanogranular Films with a High Refractive Index Matrix. *Opt. Mater. Express* **2022**, *12*, 403−413.

(41) Davoyan, A. R.; Engheta, N. Nonreciprocal Rotating Power Flow within Plasmonic Nanostructures. *Phys. Rev. Lett.* **2013**, *111*, No. 047401.

(42) Wang, Z.; Fan, S. Optical Circulators in Two-Dimensional Magneto-Optical Photonic Crystals. *Opt. Lett.* **2005**, *30*, 1989−1991.

(43) Wang, Z.; Fan, S. Magneto-Optical Defects in Two-Dimensional Photonic Crystals. *Appl. Phys. B* **2005**, *81*, 369−375.

(44) Jackiw, R.; Rebbi, C. Solitons with Fermion Number 1/2. *Phys. Rev. D* **1976**, *13*, No. 3398.

(45) Gorlach, A. A.; Zhirihin, D. V.; Slobozhanyuk, A. P.; Khanikaev, A. B.; Gorlach, M. A. Photonic Jackiw-Rebbi States in All-Dielectric Structures Controlled by Bianisotropy. *Phys. Rev. B* **2019**, *99*, No. 205122.

(46) Kim, M.; Rho, J. Quantum Hall Phase and Chiral Edge States Simulated by a Coupled Dipole Method. *Phys. Rev. B* **2020**, *101*, No. 195105.

(47) Fukui, T.; Hatsugai, Y.; Suzuki, H. Chern Numbers in Discretized Brillouin Zone: Efficient Method of Computing (Spin) Hall Conductances. *J. Phys. Soc. Japan* **2005**, *74*, 1674−1677.

(48) Wang, C.; Zhang, H.; Yuan, H.; Zhong, J.; Lu, C. Universal Numerical Calculation Method for the Berry Curvature and Chern Numbers of Typical Topological Photonic Crystals. *Front. Optoelectron.* **2020**, *13*, 73−88.

(49) Skirlo, S. A.; Lu, L.; Soljačić, M. Multimode One-Way Waveguides of Large Chern Numbers. *Phys. Rev. Lett.* **2014**, *113*, No. 113904.

https://doi.org/10.1021/acsphotonics.1c01942
ACS Photonics 2022, 9, 1621−1626